Journal of Solid State Electrochemistry (2019) 23:1697–1703
https://doi.org/10.1007/s10008-019-04275-9

ORIGINAL PAPER

Electrospun tin-carbon nanocomposite as anode material for all solid state lithium-ion batteries

Fabio Maroni[1] · Pantaleone Bruni[1] · Naoki Suzuki[2] · Yuichi Aihara[2] · Fausto Croce[1]

Received: 7 February 2019 / Revised: 2 April 2019 / Accepted: 9 April 2019 / Published online: 22 April 2019

Abstract

All-solid-state batteries represent the next generation of electrochemical energy storage systems. A tin-carbon nanocomposite material is prepared by the electrospinning technique and employed as candidate anode material in such devices. The as-prepared material has been structurally and morphologically characterized. The electrochemical characterization of the Sn(nano)/C composite showed also good electrochemical reversibility, and stability upon 100 galvanostatic cycle experiments with a quite stable interface, as highlighted by impedance spectroscopy experiments.

Keywords Tin · Electrospinning · Alloying · All-solid-state · Lithium batteries

Introduction

Nowadays, lithium-ion batteries (LIBs) are the most widespread and efficient way to electrochemically store energy [1]. Their wide range of applications, from smartphone to laptops and recently in electric vehicles (EVs), poses different challenges in terms of energy density, eco-friendliness, and overall, safety [2]. The current LIB technology employs a liquid electrolyte (LE) solution of organic and flammable carbonate solvents in which a fluorinated lithium salt is dissolved, which poses a potential safety and environmental risk in high energy density battery packs [3]. In this regard, much attention has been recently devoted to the study and development of new high-performance all-solid-state lithium-ion batteries (ASLBs) [4, 5] which differently from traditional LIBs, make use of a solid electrolyte (SE), considerably safer and lighter than a liquid system [6]. In this view, current research is focused on several classes of solid lithium-ion conductors with conductivities up to 10^{-4}–10^{-3} S cm^{-1} at room temperature, versus a higher 10^{-2} S cm^{-1} conductivity value for traditional LE systems [7]. Among them, solid oxides like perovskite-type phases [8], NASICON [9], and garnet type [10]-related structures have been studied. Despite this, solid oxides are brittle and their handling is not easy. On the other hand, the Li_2S/P_2S_5 system, among other sulfide electrolytes, cannot be handled in air due to reaction with ambient H_2O with the generation of poisonous H_2S [11, 12]. But, given its high ionic conductivity, up to 10^{-3} S cm^{-1} [13] and the possibility to be handled and cold-pressed at room temperature thanks to their higher deformability pose a valid alternative to solid oxide electrolytes which require more drastic handling conditions [14]. Electrode materials already employed in LE systems need to be reinvestigated in light of a different and critical solid electrolyte/active material interface in ASLBs [15], and new approaches need to be thought and envisaged. Graphite still represents the industry standard with its 372 mAh g^{-1} theoretical specific capacity [16], but both in LEs and ASLBs higher energy densities are needed to meet market expectations. In this regard, several alternative chemistries for anode materials have been proposed, like alloying materials (Sn, Si) [17] that ensure a fairly flat and relatively low working voltage Vs Li^+/Li couple, and very high theoretical capacities. Despite this, alloying materials suffer from several disadvantages that need to be overcome in order to make them feasible in a commercial cell: a huge volume variation (up to 300%) upon (de)lithiation which cause pulverization, loss of contact and cell failure, and low electronic conductivities which hamper kinetic properties.

Electronic supplementary material The online version of this article (https://doi.org/10.1007/s10008-019-04275-9) contains supplementary material, which is available to authorized users.

✉ Fausto Croce
Fausto.croce@unich.it

[1] Department Of Pharmacy, University Of Chieti-Pescara "G. D'Annunzio", Via dei Vestini, 66100 Chieti, Italy

[2] Samsung R&D Institute Japan, Minoh-shi, Osaka 562-0036, Japan

Among alloying materials, tin with its 995 mAh g^{-1} theoretical specific capacity has been thoroughly studied [18] in LE systems and needs to be investigated also in ASLB systems.

To overcome the aforementioned issues, several strategies have been employed, from the reduction of particle size [19], to the adoption of new and innovative morphologies [20, 21], to the implementation of support carbon matrices [22–24], but often they are long time-consuming procedures coupled with the use of toxic and expensive reagents.

Among other techniques, electrospinning [25] has proved to be capable of obtaining fibrous and open morphologies with a fairly simple experimental setup and operational straightforwardness, making it viable to the preparation on innovative electrode materials [26–28].

Herein, we demonstrate the preparation, and full characterization of a new electrospun tin/carbon nanocomposite as candidate anode material in a ASLB system.

Experimental

Material synthesis

The micro-nanofiber mats were prepared through an electrospinning process. The polymer blend was prepared dissolving polyacrylonitrile (M_w = 150,000, Aldrich) and polymethylmethacrylate (M_w = 120,000, Aldrich) in a 5:1 ratio in *N*,*N*-dimethylformamide (DMF, Aldrich). The solution was stirred for 20 h at 60 °C on a heating plate. Tin nanoparticles (SkySpring Nanomaterials Inc.) were then added, dispersed by sonication for 15 min in an ultrasonic bath (S30H Elmasonic), and stirred for 1 h at room temperature. The polymeric solution was electrospun at a constant flow rate of 0.60 ml h^{-1} and with a DC voltage of 15–18 kV. The relative humidity and the environmental temperature were 20% and 30 °C, respectively. The distance between the needle and the plate collector (covered with an aluminum foil) was 15 cm, with the needle at 10° of inclination angle. It was used a glass syringe a steel needle having 0.1-mm inner diameter.

Electrospun mats were finally stabilized under air flow at 250 °C for 1 h at a heating rate of 5 °C min^{-1}. Thermal reduction was performed at 700 °C under Ar/H_2 flow (95:5, 200 ml min^{-1}) at a heating rate of 10 °C min^{-1} to 400 °C and then 5 °C min^{-1} to 700 °C with a final plateau of 3 h.

Material characterization

The electrospun Sn(nano)/C nanocomposite material has been characterized by means of X-ray diffraction using a Philips diffractometer (Cu $K\alpha$ = 1.540 Å) in Bragg-Brentano $\theta/2\theta$ geometry and Raman spectroscopy using a Horiba iHR320 spectrometer, equipped with a 660-nm laser as light source. SEM micrographs were recorded on a ZEISS LEO 1550 FE-SEM instrument, equipped with a X-MAXN EDX detector by Oxford Instruments. Thermogravimetric analysis has been performed with a Netzsch 2500 Regulus instrument, in air atmosphere, in a temperature range of 25–950 °C with a heating ramp of 10 °C min^{-1}.

Cell assembly and electrochemical measurements

Electrode powder mix was by prepared by means of ball milling at 250 rpm for 1 h of the active material, the solid-state electrolyte and carbon nanofibers (CNF) as conductive additive, in the 35 (nanocomposite):60 (solid electrolyte):5 (CNF) proportion, respectively. Solid-state torque cells were assembled in Ar-filled glovebox (MBraun): 200 mg of a (25:75) LiI/Li_2S-P_2S_5 solid-state electrolyte was weighed and cold-pressed at 1 ton to prepare a pellet, and then 5 mg of electrode powder mix was weighed and put, with a Li-In counter electrode, into the respective sides of the solid-state cell and pressed at 4 tons. The cell was tightened using a torque wrench. Active material mass loading was 1.33 mg cm^{-2}. Cyclic voltammetries, galvanostatic cycling tests, and impedance experiments have been performed with the VMP2/Z potentiostat/galvanostat (Bio-Logic) in the potential range 0.010–2.000 V. The impedance spectra were recorded at T = 25 °C, E = 2.000 V, in the frequency range 100 KHz–10 mHz with an oscillation amplitude of ± 5 mV. All the potential values are reported versus the Li^+/Li couple.

Results and discussion

Synthesis and characterization

In Fig. 1, it is briefly reported the experimental assembly of the electrospinning system used for the preparation of the Sn(nano)/C material. This technique, already used by our

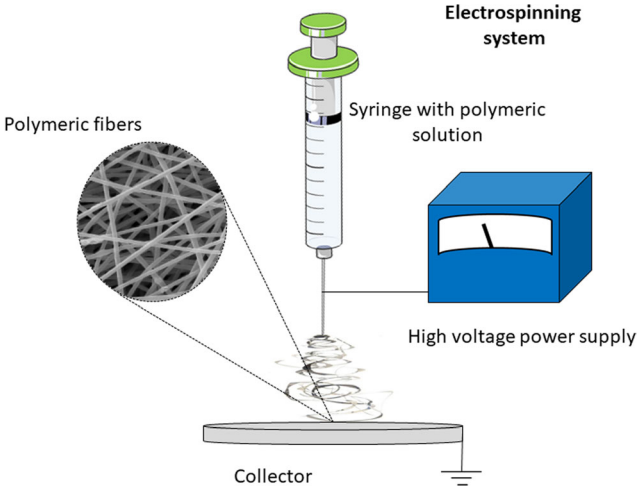

Fig. 1 Experimental electrospinning apparatus scheme

group in previous works to prepare nanostructured high-performance Li-ion anode materials [29], provides a certain degree of flexibility when it comes to tune local nanoparticle morphology to maximize performance.

In particular, the mixed polymer PAN/PMMA precursor solution, followed by a first stabilization in air atmosphere at T = 250 °C and a final annealing in Ar/H_2 atmosphere at T = 700 °C, provided a uniform and consistent fibrous carbon matrix, in which Sn metal nanoparticles are dispersed. The porosity of the carbon matrix is due to the rapid decomposition of PMMA into CO_2 during the step at T = 250 °C which leaves lots of apertures and pores in the remaining poly(acrylonitrile) matrix, which undergoes a well documented intramolecular cyclization process of nitrile (–C ≡ N) groups and a intermolecular cross-linking which stabilizes the polymer precursor network, prior to the thermal annealing step at T = 700 °C in reducing atmosphere, which yields the final conductive supporting carbon matrix [30, 31]. In addition, the stabilization process prevents the melting of the as-prepared electrospun fibers, obtaining a "precursor" conducting network which is obtained with the carbonization step.

XRD pattern of the Sn nanocomposite is shown in Fig. 2a, peaks at 30.62°, 32.03°, and 44.85° (labeled with a cross) have been indexed as [200], [101], and [211] reflection planes of metallic tin. The broad peak visible between 26° and 30° confirms for the presence of amorphous carbon due to PAN/PMMA reduction in Ar/H_2 atmosphere. In addition, SnO_2 impurities have been identified and the relative peaks labeled with an asterisk. SnO_2 presence is likely to occur due to the preparation procedure of the material, after the first thermal step at T = 250 °C in air atmosphere, in which tin metal is converted to SnO_2, and then almost completely reduced back to tin metal in the second thermal annealing in Ar/H_2 95:5 atm.

Raman spectrum, shown in Fig. 2b, reveals two very pronounced bands at 1341 cm^{-1} and 1578 cm^{-1} which represent carbon D and G bands, due to lattice vibration and carbon bond stretching, found in sp^2 carbon materials, respectively [32].

Thermogravimetric analysis, shown in Fig. 2c, carried out in air, showed a good thermal stability characterized by a 4% weight loss up to T = 200 °C mainly due to moisture and volatile species, and a second and abrupt weight loss between T = 400 °C and T = 560 °C due to conversion of the

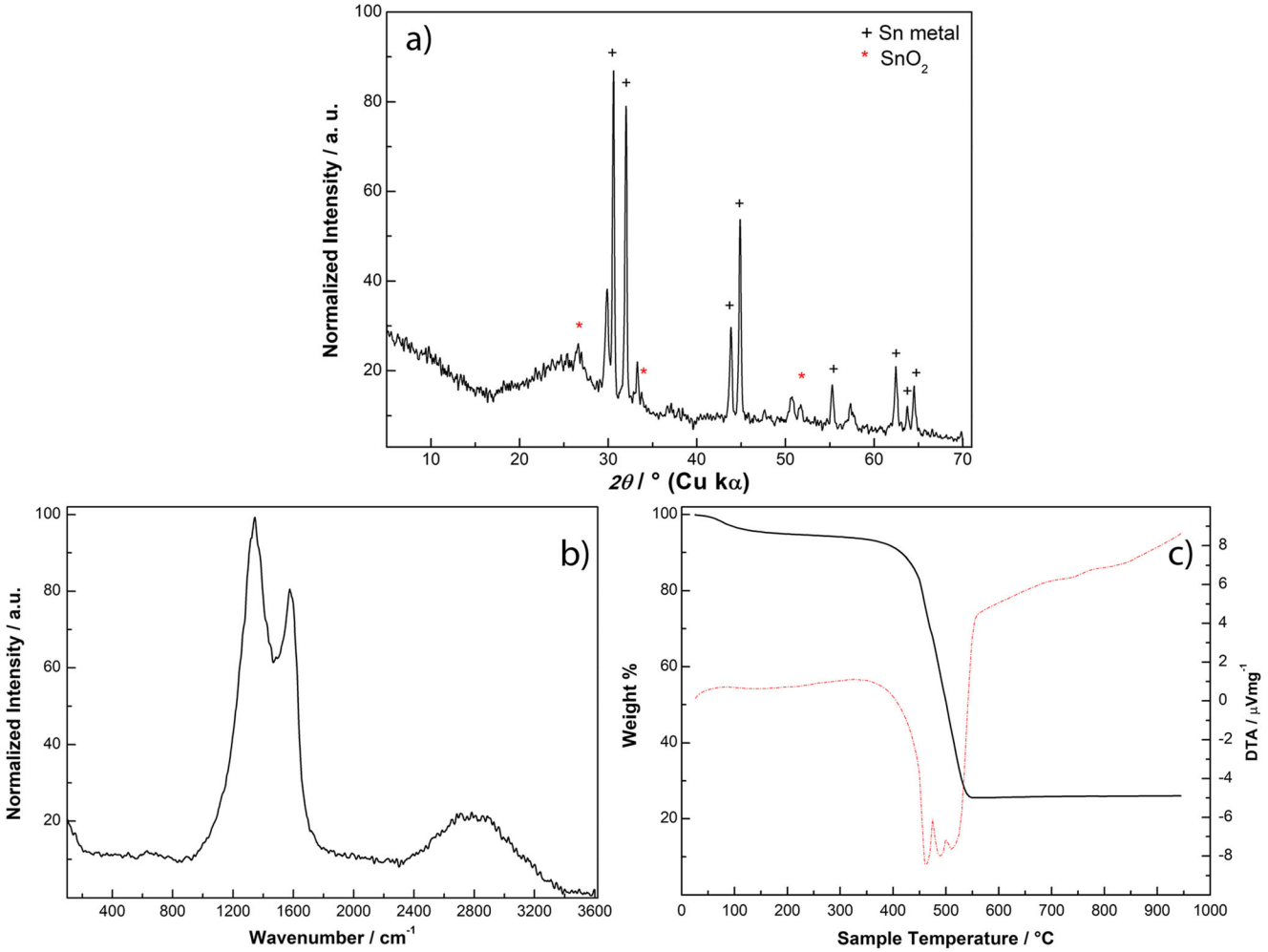

Fig. 2 **a**) Sn(nano)/C XRD pattern. **b**) Raman spectrum. **c**) TGA analysis

carbonaceous matrix to CO_2 and oxidation on metallic tin to SnO_x, for a 65% carbon content.

SEM micrographs, shown in Fig. 3a–c recorded at various magnifications, show a regular distributions of carbon fibers, with micrometer scale in length and hundreds of nanometers in width, in which Sn nanoparticles are dispersed but not easily visible.

In order to address this issue, in Fig. 3d, a backscattered electron (BSE) micrograph is shown, reporting the uniform dispersion of tin nanoparticles (bright spots) in the carbon fibers. The intimate contact between carbon fibers and tin active material enables a 3D-interconnected conducting network, for improved eletrochemical performance. The presence of any additional metallic element has been ruled out by EDX analysis.

Electrochemical characterization

Figure 4a shows the cyclic voltammetry test of the Sn(nano) material, carried out at $\upsilon = 0.050$ mV s^{-1} scan rate, which shows electrochemical features, related to Li-Sn alloying, comparable to those of traditional liquid system. The electrochemical Li-Sn alloying process usually proceeds in accord to the equation: $4.4Li^+ + 4.4e^- + Sn \rightarrow Li_{4.4}Sn$ [18]. In the cathodic area, peak A ($E = 0.97$ V) could be related to an irreversible passivation-like behavior due to both interfacial reactions of the active material with the electrolyte and the reduction of SnO_2 particles to their metallic state with the on-going formation of Li_2O [33, 34], peak B ($E = 0.67$ V) and C ($E = 0.46$ V) have been assigned to Li-Sn alloying processes, and peak D to Li-C insertion processes. On the other hand, in the anodic section, peaks labeled as E ($E = 0.100$–0.120 V) have been assigned to Li^+ extraction from graphitized carbon of CNF additive, peaks F ($E = 0.59$ V), G ($E = 0.71$ V), and H ($E = 0.78$ V) to Li-Sn dealloying processes and finally, peak I ($E = 1.01$ V) is assigned to Li extraction from the carbon matrix. This electrochemical Li^+-ion extraction at higher anodic potential has been previously reported and is related to the intrinsic nature of the carbon, addressed as low-T carbon, obtained by the $T = 700$ °C annealing step in reducing atmosphere [35, 36]. The system exhibited good reversibility during the successive cycles, as reported in Fig. S1. Since, in previous reports, the Li_2S-P_2S_5 electrolyte has been found to possibly be source of reversible capacity [37], an additional cyclic voltammetry has been performed, with SiO_2 as inactive electrochemical species, in substitution of the active material, and as reported in Fig. S2, no reversible electrochemical activity connected with Li-electrolyte reactions has been detected.

In Fig. 4b, a successive voltammetric test has been performed at higher scan rates, from $\upsilon = 0.050$ mV s^{-1} to

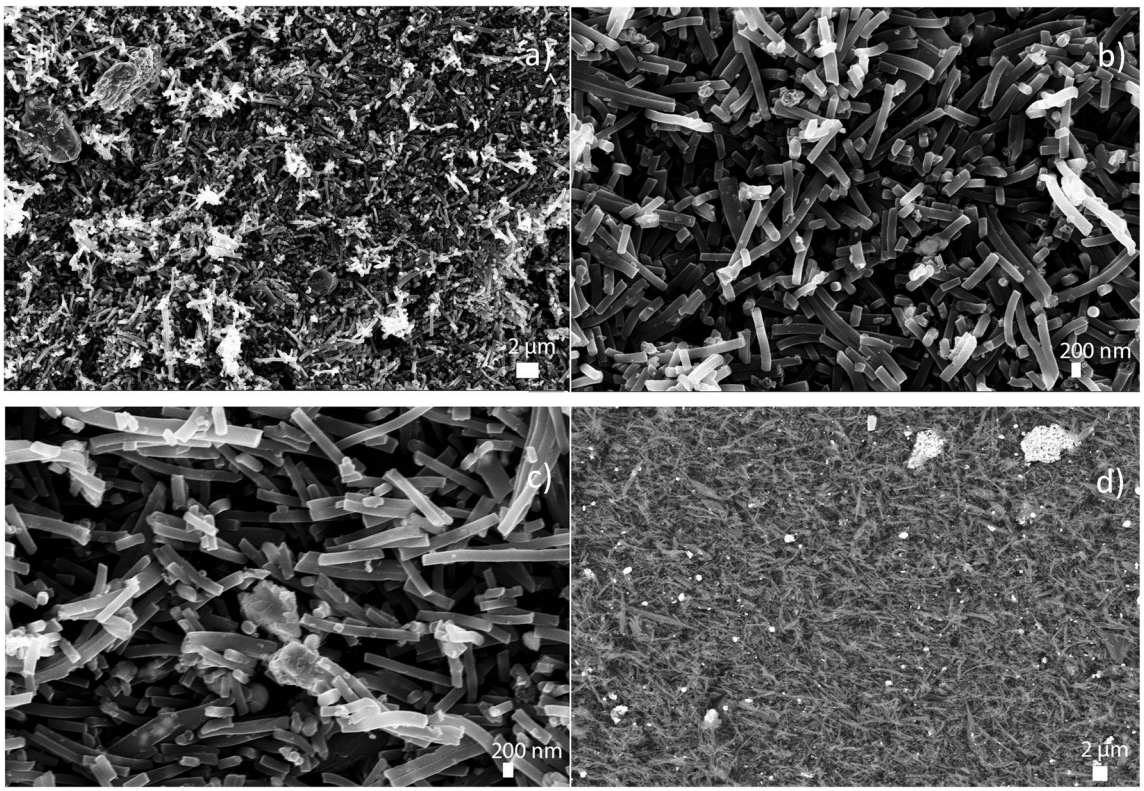

Fig. 3 **a**)–**c**) SEM micrographs recorded at different magnifications. **d**) Backscattered electrons (BSE) micrograph

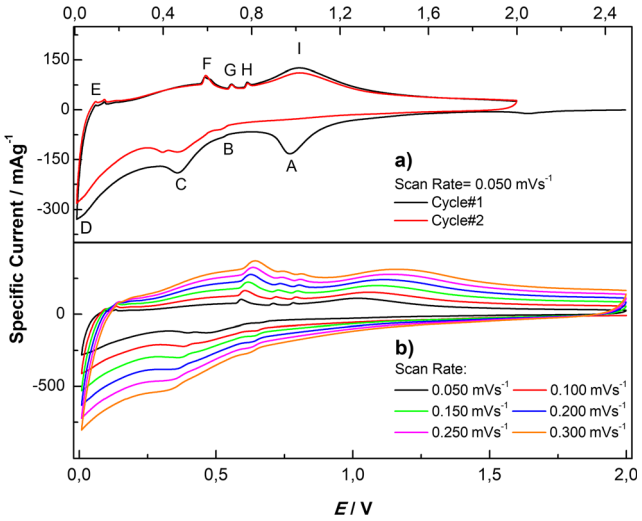

Fig. 4 **a**) Cyclic voltammetry (CV) experiment conducted at $\upsilon = 0.050$ mV s^{-1} scan rate. **b**) Cyclic voltammetry experiment at increasing scan rates 0.050 mV s^{-1} < SR < 0.300 mV s^{-1}

$\upsilon = 0.300$ mV s^{-1} revealing a good kinetic response at all the investigated scan rates. Then, to evaluate cycling performance, galvanostatic experiments have been carried out at $I_{spec} = 214$ mA g^{-1} discharge specific current and $I_{spec} = 107$ mA g^{-1} charge specific current, and the results are displayed in Fig. 5a. The first cycle is characterized by discharge capacity of 1266 mAh g^{-1} and a coulombic efficiency of 56% due to Li-Sn first cycle irreversible processes and the possible formation of an interfacial electrode-electrolyte passivation layer. The second galvanostatic cycle showed a discharge capacity of 763 mAh g^{-1} with the coulombic efficiency rising from 88% to over 99% in the successive cycles. At the end of the experiment, at cycle 100, a discharge capacity of 374 mAh g^{-1} with a final capacity retention of 49.08% highlights the promising performance of this active material in an ASLB lithium ion cell configuration.

The regular slight increase in capacity of several cycles, visible in Fig. 5a, is due to the recording a EIS spectra, which have been analyzed and showed afterwards. Since the efficiency quickly jumps to values over 99% for the remaining duration of the experiment, it could be speculated that the decrease in specific capacity during cycling can be assigned to the repeated expansion/contraction cycles of the Sn alloy, which causes mechanical degradation of particles, followed by a loss of contact with the solid electrolyte particles. Figure 5b, capacity profiles of the first galvanostatic cycle, shows a sloping plateau around $E = 1.000$ V, a second one at $E = 0.500$ V, and a continuous sloping line until the cut-off potential of $E = 0.010$ V is reached. Upon charging, a first sloping plateau is present in the $E = 0.500$ V region and a second one at $E = 1.000$ V, followed by a sloping line up to $E = 2.000$ V. Successive cycles show a very good reversibility. Differential analysis, shown in Fig. 5c, was used to investigate the electrochemical behavior of the active material during galvanostatic cycling. From the results showed in Fig. 4a, it can be seen that each one of the electrochemical features already evidenced in the cyclic voltammetry experiment is present, both in discharge (features a,b,c) and in the charge steps

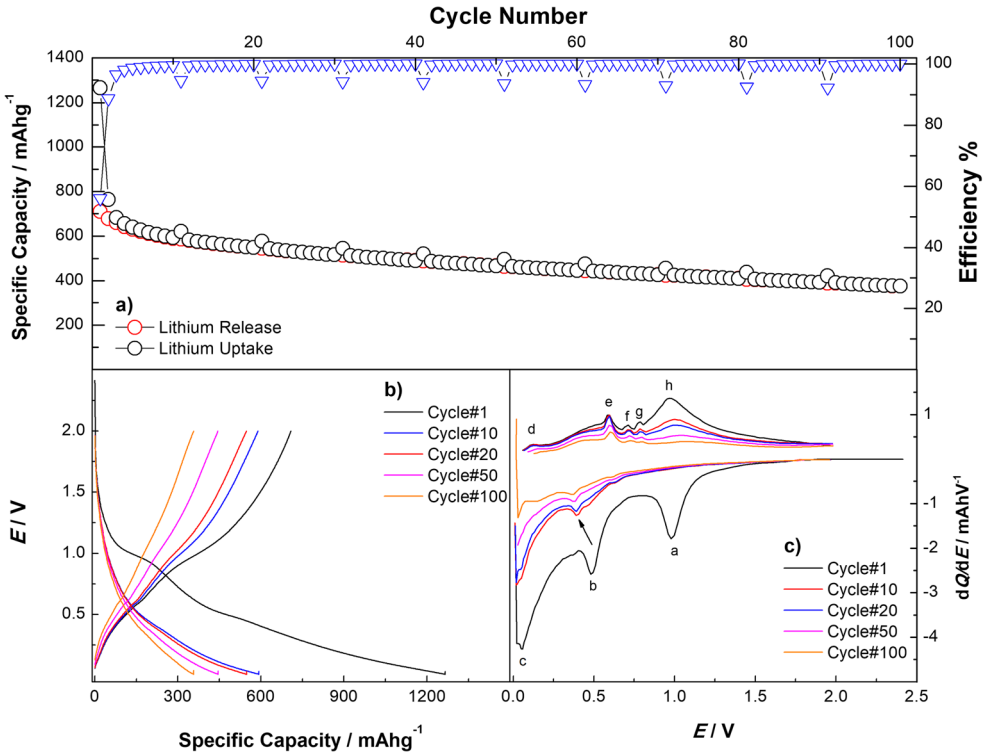

Fig. 5 **a**) Sn(nano)/C galvanostatic cycling experiment. **b**) Specific capacity profiles. **c**) Differential analysis

(features d,e,f,g,h) confirming a good reproducibility of this system, as well as its reversibility.

Electrochemical impedance spectroscopy (EIS) has been used to investigate the evolution of the interface of the ASLB during galvanostatic long cycling, and the spectrum of the first cycle is reported in Fig. 6 and its inset. Typical impedance spectrum, recorded at a fixed potential $E = 3.000$ V after 30 min of relaxation time, shows a closing semicircle at high frequency that could be tentatively assigned to the formation of an additional interface like a passivation layer, a broad semicircle at medium-to-low frequencies due to charge-transfer phenomena and a sloping line a low frequencies due to diffusive processes.

In Fig. S3 is reported the evolution of the interface through the overlay of selected cycles, in which is visible a stabilization of the interface from cycle 50 up to cycle 100. Finally, to give a quantitative insight of resistance values, impedance spectra were fitted by Boukamp software [38], using the equivalent circuit shown in Fig. S4. The circuit is characterized by a resistive element labeled as R_{SSE} due to the resistance of the electrolyte, followed by a parallel between a resistive element labeled as R_{pl} assigned to the formation of a passivation layer, and a capacitive element labeled as C_{pl} due to capacitance of the passivation layer. Then, there is a second parallel between a resistive element, which has been labeled as R_{Ct}, due to charge-transfer resistance, and a capacitive element, labeled as C_{dl}, due to the formation of an electric double layer. Finally, a constant phase element (CPE) has been assigned as an impedance element due to diffusive processes. Numerical values of the circuit elements are reported in Table S1 and plotted in Fig. S5. Looking at the plotted resistance values vs. cycle, it is visible a very stable trend in the interface, with a slight increase in electrolyte resistance R_{SSE}, probably due to its consumption for the formation of a passivation layer, which, in turn, shows a very good stability (R_{pl}) throughout all the experiment. Charge-transfer resistance values (R_{Ct}) also show good stability, after an initial increase. The globally stable resistance values are in good accordance with the recorded impedance spectra.

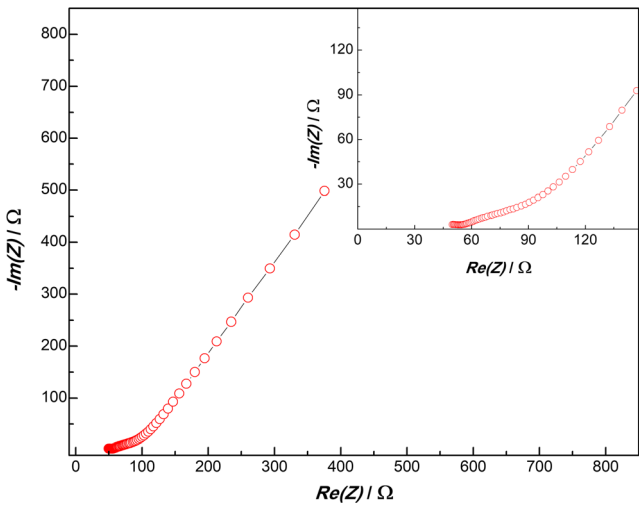

Fig. 6 Electrochemical impedance spectroscopy experiment—impedance spectrum of cycle 1

Conclusion

In conclusion, an electrospun Sn metal/carbon nanocomposite anode material for all-solid-state lithium batteries using a sulfide electrolyte has been prepared from Sn metal nanoparticles dispersed in PAN/PMMA polymer blend as both carbon source and supporting matrix. It has been morphologically and structurally characterized by several experimental techniques, which confirmed both morphology and the retention of the metal nature of the Sn nanoparticles during the nanocomposite preparation.

Electrochemical characterization showed all the typical features arising from Li-Sn alloying processes in the cyclic voltammetry experiment, which were then confirmed by differential analysis of selected cycles of a galvanostatic experiment. Cyclic voltammetry experiments using an inactive electrochemical material like SiO_2 excluded the contribution in capacity by the solid-state electrolyte. Good cycling performance showed a capacity retention of 66.67% after 50 galvanostatic cycles and above 300 mAh g^{-1}. Finally, impedance spectroscopy revealed the possible presence of a passivation layer, and at the same time, a very stable interface during a long cycling experiment, with resistance values quantified by fitting the equivalent circuit elements.

Acknowledgments This work was carried out within a joint research project between the University of Chieti and Samsung SRJ at Minoh-Shi, Japan. The author wants to thank Dr. Gabriele Giuli for the XRD patterns, Dr. Laura Petetta for the SEM micrographs, and Dr. Matteo Ciambezi at the University of Camerino for the Raman Spectra.

References

1. Scrosati B, Garche J (2010) Lithium batteries: status, prospects and future. J Power Sources 195(9):2419–2430
2. Wen J, Yu Y, Chen C (2012) A review on lithium-ion batteries safety issues: existing problems and possible solutions. Mater Express 2(3):197–212
3. Lu L, Han X, Li J, Hua J, Ouyang M (2013) A review on the key issues for lithium-ion battery management in electric vehicles. J Power Sources 226:272–288
4. Kim JG, Son B, Mukherjee S, Schuppert N, Bates A, Kwon O, Choi MJ, Chung HY, Park S (2015) A review of lithium and non-lithium based solid state batteries. J Power Sources 282:299–322
5. Sun C, Liu J, Gong Y, Wilkinson DP, Zhang J (2017) Recent advances in all-solid-state rechargeable lithium batteries. Nano Energy 33:363–386
6. Li F, Kitaura H, Zhou H (2013) The pursuit of rechargeable solid-state Li-air batteries. Energy Environ Sci 6(8):2302–2311

7. Xu K (2004) Nonaqueous liquid electrolytes for lithium-based rechargeable batteries. Chem Rev 104(10):4303–4417
8. Stramare S, Weppner W (1999) Structural and conductivity investigations of doped Li-titanates. Ionics (Kiel) 5(5-6):405–409
9. Knauth P (2009) Inorganic solid Li ion conductors: an overview. Solid State Ionics 180(14-16):911–916
10. Thangadurai V, Narayanan S, Pinzaru D (2014) Garnet-type solid-state fast Li ion conductors for Li batteries: critical review. Chem Soc Rev 43(13):4714–4727
11. Ohtomo T, Hayashi A, Tatsumisago M, Kawamoto K (2013) Suppression of H_2S gas generation from the $75Li_2S{\cdot}25P_2S_5$ glass electrolyte by additives. J Mater Sci 48(11):4137–4142
12. Muramatsu H, Hayashi A, Ohtomo T, Hama S, Tatsumisago M (2011) Structural change of Li_2S-P_2S_5 sulfide solid electrolytes in the atmosphere. Solid State Ionics 182(1):116–119
13. Ohtomo T, Hayashi A, Tatsumisago M, Kawamoto K (2013) Glass electrolytes with high ion conductivity and high chemical stability in the system LiI-Li_2O-Li_2S-P_2S_5. Electrochemistry 81(6):428–431
14. Ren Y, Chen K, Chen R, Liu T, Zhang Y, Nan CW (2015) Oxide electrolytes for lithium batteries. J Am Ceram Soc 98(12):3603–3623
15. Li Y, Zhou W, Chen X, Lü X, Cui Z, Xin S, Xue L, Jia Q, Goodenough JB (2016) Mastering the interface for advanced all-solid-state lithium rechargeable batteries. Proc Natl Acad Sci 113(47):13313–13317
16. Nazri GA, Pistoia G (2003) Lithium batteries - science and technology. Springer US, Boston
17. Zhang WJ (2011) A review of the electrochemical performance of alloy anodes for lithium-ion batteries. J Power Sources 196(1):13–24
18. Obrovac MN, Chevrier VL (2014) Alloy negative electrodes for Li-ion batteries. Chem Rev 114(23):11444–11502
19. Gaberscek M, Dominko R, Jamnik J (2007) Is small particle size more important than carbon coating? An example study on LiFePO4 cathodes. Electrochem Commun 9(12):2778–2783
20. Wang C, Fang D, Wang H et al (2016) Uniform nickel vanadate ($Ni_3V_2O_8$) nanowire arrays organized by ultrathin nanosheets with enhanced lithium storage properties. Sci Rep 6(1):20826
21. Cui LF, Yang Y, Hsu CM, Cui Y (2009) Carbon-silicon core-shell nanowires as high capacity electrode for lithium ion batteries. Nano Lett 9(9):3370–3374
22. Wang D, Yang J, Li X, Geng D, Li R, Cai M, Sham TK, Sun X (2013) Layer by layer assembly of sandwiched graphene/SnO_2 nanorod/carbon nanostructures with ultrahigh lithium ion storage properties. Energy Environ Sci 6(10):2900
23. Li X, Zhang Y, Li T, Zhong Q, Li H, Huang J (2014) Carbon encapsulated ultrasmall SnO_2 nanoparticles anchoring on graphene/TiO2 nanoscrolls for lithium storage. Electrochim Acta 147:40–46
24. Liu H, Chen S, Wang G, Qiao SZ (2013) Ordered mesoporous core/shell SnO_2/C nanocomposite as high-capacity anode material for lithium-ion batteries. Chem - A Eur J 19(50):16897–16901
25. Xue J, Xie J, Liu W, Xia Y (2017) Electrospun nanofibers: new concepts, materials, and applications. Acc Chem Res 50(8):1976–1987
26. Ban C, Chernova NA, Whittingham MS (2009) Electrospun nano-vanadium pentoxide cathode. Electrochem Commun 11(3):522–525
27. Teh PF, Pramana SS, Sharma Y, Ko YW, Madhavi S (2013) Electrospun $Zn_{1-x}Mn_xFe_2O_4$ nanofibers as anodes for lithium-ion batteries and the impact of mixed transition metallic oxides on battery performance. ACS Appl Mater Interfaces 5(12):5461–5467
28. Mai L, Xu L, Han C, Xu X, Luo Y, Zhao S, Zhao Y (2010) Electrospun ultralong hierarchical vanadium oxide nanowires with high performance for lithium ion batteries. Nano Lett 10(11):4750–4755
29. Meschini I, Nobili F, Mancini M, Marassi R, Tossici R, Savoini A, Focarete ML, Croce F (2013) High-performance Sn@carbon nanocomposite anode for lithium batteries. J Power Sources 226:241–248
30. Gergin I, Ismar E, Sarac AS (2017) Oxidative stabilization of polyacrylonitrile nanofibers and carbon nanofibers containing graphene oxide (GO): a spectroscopic and electrochemical study. Beilstein J Nanotechnol 8:1616–1628
31. Alarifi IM, Khan WS, Asmatulu R (2018) Synthesis of electrospun polyacrylonitrile-derived carbon fibers and comparison of properties with bulk form. PLoS One 13:1–14
32. Ferrari AC, Basko DM (2013) Raman spectroscopy as a versatile tool for studying the properties of graphene. Nat Nanotechnol 8(4):235–246
33. Birrozzi A, Raccichini R, Nobili F, Marinaro M, Tossici R, Marassi R (2014) High-stability graphene nano sheets/SnO_2 composite anode for lithium ion batteries. Electrochim Acta 137:228–234
34. Lian P, Wang J, Cai D, Ding L, Jia Q, Wang H (2014) Porous SnO_2@C/graphene nanocomposite with 3D carbon conductive network as a superior anode material for lithium-ion batteries. Electrochim Acta 116:103–110
35. Dahn JR, Zheng T, Liu Y, Xue JS (1995) Mechanisms for lithium insertion in carbonaceous materials. Science (80-) 270(5236):590–593
36. Zheng T, Xue JS, Dahn JR (1996) Lithium insertion in hydrogen-containing carbonaceous materials. Chem Mater 8(2):389–393
37. Aihara Y, Ito S, Omoda R et al (2016) The electrochemical characteristics and applicability of an amorphous sulfide-based solid ion conductor for the next-generation solid-state lithium secondary batteries. Front Energy Res 4:1–8
38. Boukamp BA (1986) A nonlinear least squares fit procedure for analysis of immittance data of electrochemical systems. Solid State Ionics 20(1):31–44